Research in Astron. Astrophys. **2012** Vol. **X** No. **XX**, 000–000
http://www.raa-journal.org *http://www.iop.org/journals/raa*

***R**esearch in*
***A**stronomy and*
***A**strophysics*

arXiv:1403.7954v1 [astro-ph.SR] 31 Mar 2014

Photometric Investigation of the K-type Extreme-Shallow Contact Binary V1799 Orion *

Nian-Ping Liu[1,2,3], Sheng-Bang Qian[1,2,3], Wen-Ping Liao[1,2], Jia-Jia He[1,2], Er-Gang Zhao[1,2], Liang Liu[1,2]

[1] Yunnan Observatories, Chinese Academy of Sciences, Kunming, 650011 China; *lnp@ynao.ac.cn*
[2] Key Laboratory for the Structure and Evolution of Celestial Objects, Chinese Academy of Sciences, 650011 Kunming, China
[3] University of Chinese Academy of Sciences, Beijing 100049, China

Received ; accepted

Abstract New multi-color light curves of the very short period K-type eclipsing binary V1799 Ori were obtained and analyzed with the W-D code. The photometric solutions reveal that the system is a W-type shallow-contact binary with a mass ratio of $q = 1.335(\pm0.005)$ and a degree of contact about $f = 3.5(\pm1.1)\%$. In general, the results are in good agreement with which is reported by Samec. The remarkable O'Connell effects in the light curves are well explained by employing star spots on the binary surface, which confirms that the system is active at present. Several new times of light minimum were obtained. All the available times of light minimum were collected, along with the recalculated and new obtained. Applying a least-squares method to the constructed O-C diagram, a new ephemeris was derived for V1799 Ori. The orbital period is found to show a continuous weak increase at a rate of $1.8(\pm0.6) \times 10^{-8}$ days·yr^{-1}. The extreme-shallow contact, together with the period increase, suggests that the binary may be at a critical stage predicted by the TRO theory.

Key words: binaries : close – binaries : eclipsing – stars: individual (V1799 Ori)

1 INTRODUCTION

The K-type short-period contact binaries, especially those with periods shorter than 0.3 days, are most probably main-sequence objects and mostly convective (Bradstreet 1985). They belong to W UMa type binaries which both components share common envelope that lying between the inner and outer critical Roche-lobe surfaces. W UMa type binaries have been divided into two sub-groups: A-type and W-type according to Binnendijk (1970). Generally speaking, the A-type systems are more likely to have earlier spectral type than the W-type systems (Rucinski 1974). So it is supposed that a large amount of K-type short-period contact binaries may be W-type systems. The majority of W-type contact binaries show shallow contact characteristics (Zhu et al. 2010; He 2009 PhD). Therefore, they are good targets for testing the thermal relaxation oscillation theory (TRO theory; eg., Lucy 1976; Flannery 1976; Robertson & Eggleton 1977)

V1799 Orion, or V1799 Ori (=GSC 00096-00175, $\alpha_{2000.0} = 04^h47^m18^s.19$ and $\delta_{2000.0} = +06^\circ40'56''.1$) is a very short period (with period shorter than 0.3 days) eclipsing binary. It was first suspected to show variability by Hanley & Shapley (1940) (the cross identification is HV 10397). However,

∗ Supported by the National Natural Science Foundation of China.

Table 1 Summary of the multi-color light curves

Wave Band	min.I-min.II (mag.)	max.(0.25)-max.(0.75) (mag.)	min.I-max.(0.75) (mag.)
B	0.15	0.05	1.08
V	0.18	0.04	1.03
R	0.13	0.03	0.98
I	0.10	0.03	0.93

it had been neglected for a long time until ROSTE survey (Akerlof et al. 2000) rediscovered it to be a eclipsing binary with EW type light curves (Khruslove 2006) (the cross identification is NSV 1719). The following ephemeris was reported (Khruslove 2006):

$$\mathrm{Min.I(HJD)} = 2451524.829 + 0^{\mathrm{d}}.29031 \times E. \quad (1)$$

It was then monitored many times by several researchers such as Diethelm (2009, 2010, etc.) and Nelson (2010). Recently, The O-C gateway (http://var.astro.cz/ocgate/) gave out a more exact ephemeris,

$$\mathrm{Min.I(HJD)} = 2451524.829 + 0^{\mathrm{d}}.290304 \times E. \quad (2)$$

The first photometric analysis of V1799 Ori was given by Samec et al. (2010) as a student/professional collaborative program. Their photometric solutions depicted V1799 Ori as a W-type, extremely shallow-contact, eclipsing binary. The degree of contact factor $3\,\%$ is rather exceptional. Their solutions uncovered two hot spots on the components, which indicates the system is quite active at present.

In this paper, we present the analysis of newly obtained complete CCD light curves and compare the results with those given by Samec et al. Especially, we carry out a more exact period investigation of this system, using all the available times of light minimum.

2 OBSERVATIONS

New CCD photometric observations of V1799 Ori in BV(RI)$_{\mathrm{c}}$ bands were carried out on December 15, 2012 with the 1.0-m reflecting telescope at Yunnan Observatory of Chinese Academy of Sciences. An Andor DW436 2K CCD camera equiped in Cassegrain-focus was used. A standard Johnson-Cousins-Bessel filter system built on the primary focus (Zhou et al. 2009) was used. The effective field of view was $7.3' \times 7.3'$. The integration times for each image were 40 s, 30 s, 15 s and 10 s in B, V, R, and I bands, respectively. The stars 2MASS J04472543+0641432 and 2MASS J04472765+0638427 near the target were chosen as the comparison and the check stars, respectively. Their brightness and color are similar to that of the variable. The raw images were reduced with PHOT (magnitudes measurements for a list of stars) task of the aperture photometry package IRAF. Complete BVRI light curves were obtained and the original data of the light curves are listed in Tables A.1-A.4. The phased light curves are displayed in Figure 1. The phases were calculated with respect to the following ephemeris,

$$\mathrm{Min.I(HJD)} = 2456277.10109 + 0^{\mathrm{d}}.290304 \times E. \quad (3)$$

The initial epoch in this equation is the averaged time of min I (see Table 2, data with Hel. JD $2456277 \sim$). Some information about the light curves are listed in Table 1 to describe their main features. By the way, more CCD observations of V1799 Ori were made on two nights in 2013 December with the same telescope. These data were obtained around the eclipsing times and were used to determine the times of light minimum (see Table 2).

The light curves displayed in Figure 1 show remarkable O'Connell effects (different heights of light maximum, see O'Connell 1951a,b, Milone 1968), which we should taken into account in deriving photometric solutions. The two deep eclipses of the light curves will help us to derive more reliable parameters of the binary. Using a least-square parabolic fitting method, the new times of CCD light minimum were determined and are listed in Table 2.

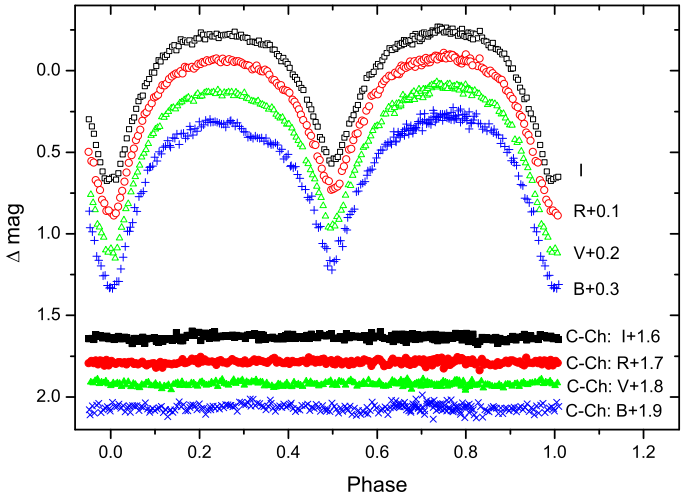

Fig. 1 Multi-color light curves of V1799 Ori obtained in 2012.

Table 2 New times of CCD light minimum.

JD (Hel.)	Error (days)	Min.	Filter	NA
2456277.10131	0.00033	I	B	35
2456277.10091	0.00030	I	I	29
2456277.10110	0.00032	I	R	34
2456277.10105	0.00030	I	V	30
2456277.24598	0.00043	II	B	36
2456277.24612	0.00031	II	I	29
2456277.24600	0.00034	II	R	29
2456277.24648	0.00033	II	V	30
2456645.20608	0.00013	I	N	54
2456657.25337	0.00012	II	I	32
2456657.25374	0.00016	II	N	32

Notes: NA is the total number of data used to determine the times of light minimum.

3 ORBITAL PERIOD INVESTIGATION OF V1799 ORI

Times of light minimum are very useful material for the orbital period study of eclipsing binaries. Therefore, we collected all the available times of light minimum in the help of O-C gateway[1]. They are listed in Table 3. Several times of light minimum from the INTEGRAL Optical Monitoring Camera (Alfonso-Garzón et al. 2012) Archive and ROTSE-I (Akerlof et al. 2000) are also listed. They are recalculated by folding the original data according to the period and applying a least-square parabolic fitting method to the eclipsing part of the folded light curves. The resulted times are actually the average times of light minimum for each group of data. The HJD times of the light minimum determined from the light curves observed by Samec et al. (2010) were reprocessed according to their observation time.

The collection of times of light minimum from literature or from reprocessed data are listed in Table 3. The O-C values calculated with respect to Equation (2) are shown in Figure 2 along with the epochs (data with errors larger than 0.001 days were not used). Seen from upper panel of Figure 2, the general

[1] http://var.astro.cz/ocgate/

Table 3 Collection of published or reprocessed times of light minimum

JD. Hel. 2,400,000+	Err. (days)	Epoch	O-C (days)	Min	Method	Ref.	Notes
51524.10538	4.8E-4	-2.5	0.00214	II	ccd	(1)	reproc
51526.28195	3.5E-4	5	0.00143	I	ccd	(1)	reproc
53591.5061	0.003	7119.0	0.00295	I	V	(2)	newp, unused
53591.6487	0.002	7119.5	0.00034	II	V	(2)	newp, unused
54014.0306	0.003	8574.5	-0.01008	II	V	(2)	newp, unused
54530.3413	0.001	10353.0	-0.00502	I	V	(2)	newp
54756.9226	9E-4	11133.5	-0.00598	II	B	(3)	
54821.66301	1.6E-4	11356.5	-0.00337	II	BVRI	(4)	reproc
54821.80835	2.9E-4	11357.0	-0.00318	I	BVRI	(4)	reproc
54822.67936	2.1E-4	11360.0	-0.00308	I	BVRI	(4)	reproc
54822.82433	4.2E-4	11360.5	-0.00326	II	VRI	(4)	reproc
54824.71134	1.4E-4	11367.0	-0.00323	I	BVRI	(4)	reproc
54824.85607	7.1E-4	11367.5	-0.00365	II	V	(4)	reproc
54827.76016	2.2E-4	11377.5	-0.00260	II	BVR	(4)	reproc
54827.90541	1.5E-4	11378.0	-0.00250	I	BVR	(4)	reproc
55113.8532	5E-4	12363.0	-0.00415	I	ccd	(5)	
55135.7727	4E-4	12438.5	-0.00260	II	V	(6)	
55135.9187	5E-4	12439.0	-0.00176	I	V	(6)	
55506.9248	3E-4	13717.0	-0.00417	I	V	(7)	
55937.5900	0.003	15200.5	-0.00495	II	V	(8)	unused
55937.7353	8E-4	15201.0	-0.00480	I	V	(8)	
56237.9093	8E-4	16235.0	-0.00514	I	V	(9)	

Notes: ROTSE-I data can be retrieved in the NSVS database (http://skydot.lanl.gov/nsvs/nsvs.php). newp = Based on data from the OMC Archive at CAB (INTA-CSIC), pre-processed by ISDC, times of light minimum are newly calculated; reproc = data were reprocessed.

References: (1) Khrus1ov 2006; (2) present paper; (3)Diethelm 2009; (4)Samec et al. 2010; (5)Nelson 2010; (6) Diethelm 2010; (7) Diethelm 2011; (8) Diethelm 2012; (9) Diethelm 2013.

trend of the O-C shows a upward parabolic change without overlapping an obvious cyclic oscillation. By using a weighted least square method, a new ephemeris was derived to be

$$\begin{aligned}\mathrm{Min.I(HJD)} = \; & 2451524.8307(\pm 0.0003) + 0^{\mathrm{d}}.29030351(\pm 0.00000005) \times E \\ & +7^{\mathrm{d}}.0(\pm 2.4) \times 10^{-12} \times E^2.\end{aligned} \tag{4}$$

The quadratic term in Equation (4) denotes a continuous period increase at a rate of $\mathrm{d}P/\mathrm{d}t = 1.8(\pm 0.6) \times 10^{-8}$ days·yr^{-1}. The residuals are also displayed in the lower panel of Figure 2. As shown in this figure, a few data point are not fitted well. It may be caused by occasional factors which would impact the shape of the light curves and therefore the determination of times of light minimum, e.g. the occurrence of solar-like activities and the unstable weather conditions. Nevertheless, the general trend of O-C data is well described by the upward parabolic fit.

By the way, a revised linear ephemeris was calculated to be

$$\mathrm{min.I(HJD)} = 2451524.8303(\pm 0.0002) + 0^{\mathrm{d}}.29030364(\pm 0.00000002) \times E, \tag{5}$$

which can be used as a preliminary prediction of times of light minimum.

4 PHOTOMETRIC SOLUTIONS WITH THE W-D METHOD

The light curves displayed in Figure 1 show EW-type variation and deep eclipsing feature in both minimum. We can predict a high orbital inclination of the binary system, which enables a reliable photometric parameter determination. To understand the geometrical structure and evolutionary state, the multi-color light curves were analyzed with the W-D method (Wilson & Devinney 1971; Wilson 1979, 1990, 1994; Wilson & van Hamme 2003). The temperature for star 1 (the star eclipsed at primary light

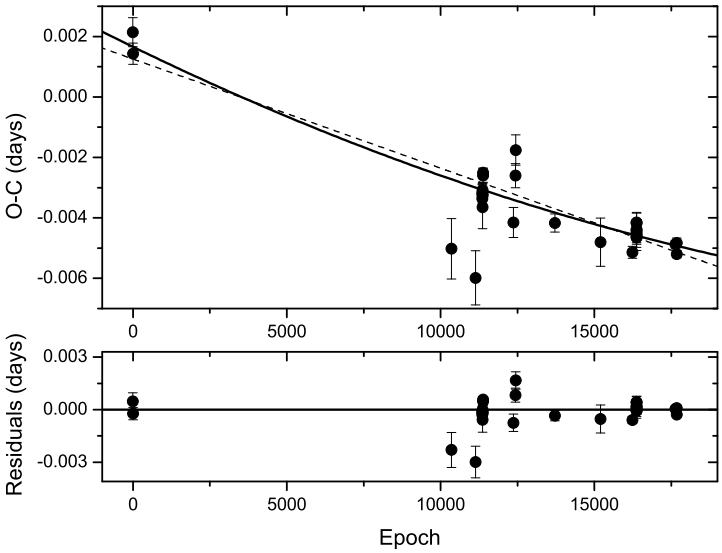

Fig. 2 Upper panel: the O-C diagram calculated using the linear ephemeris in Equation 2. The solid line refers to the upward parabolic variation, while the the dash line refers to a linear correction for the ephemeris. Low panel: the residuals after the parabolic variation was removed.

minimum) was fixed as $T_1 = 5000$ K according to Samec et al. (2010). This is reasonable because the 2MASS color index $J - H = 0.448$ and $H - K = 0.089$ given in VizieR database correspond to a K0-K2 spectral type according to Allen's table (Cox 2000). The component eclipsed at the primary light minimum are usually the hotter one so that we adopted the same temperature as Samec chose. The gravity-darkening coefficients were assumed as $g_1 = g_2 = 0.32$ (Lucy 1967) and the bolometric albedo as $A_1 = A_2 = 0.5$ (Ruciński 1969). Bolometric and bandpass square-root limb-darkening parameters are taken from van Hamme (1993). Mode 3 (contact model)was assumed during process of calculation. The adjustable parameters were: the orbital inclination i; the mean temperature of star 2, T_2; the monochromatic luminosity of star 1, L_{1B}, L_{1V}, L_{1R} and L_{1I}; and the dimensionless potential ($\Omega_1 = \Omega_2$ for mode 3).

A q-search method was used in order to get the initial input parameters. A series of mass ratios ranging from less than 0.3 to larger than 3 were assumed as trial values. Calculation were carried out with these mass ratios. The resulted sum of weighted square deviations ($\Sigma w_i(O-C)_i^2$) along with mass ratios are plotted in Figure 3. The smallest Σ was achieved at $q = 1.3$ ($q = M_2/M_1$). Then, we treated q as an an adjustable parameter and chose $q = 1.3$ as the initial value. we treated q as an an adjustable parameter and chose $q = 1.3$ as the initial value and finally a set of converged solutions were obtained.

The obtained photometric solutions are listed in Table 5 (see column 2). However, the theoretical light curves obtained does not fit the observations very well because of the obvious asymmetry in the light curves. This is the so-called O'Connell effects. Therefore, we tried to employ star spots in the model. It should be noted that the spots would be cool spots, just like sunspots, or would be hot spots, which are hotter areas on the components. Since the masses of the components are close to each other ($q = M_2/M_1 \sim 1.3$), both of them may have the possibility of producing spots. To simplify the problem, we tried adding single spot on the binary system. Together with the non-spot model, there are five scenarios to compare, which are listed in Table 4. The values in column 2 are the sum of weighted

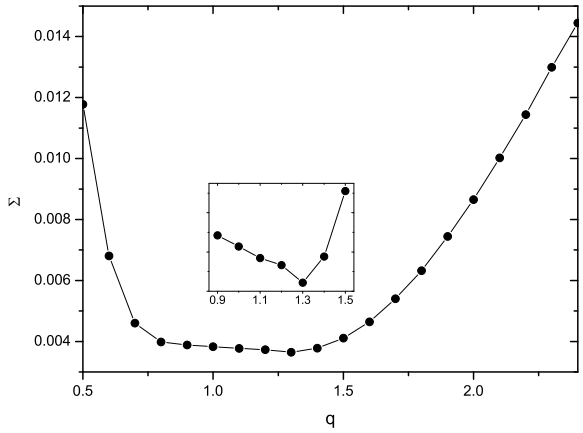

Fig. 3 Σ - q curves for V1799 Ori. Insert: a enlarged figure to show small part.

Table 4 Comparison of different spot scenarios.

Model	Spot type	$\Sigma w_i(O-C)_i^2 \times 10^3$
0	Non-spot	2.854
1	cool spot on C1	2.191
2	cool spot on C2	2.255
3	hot spot on C1	1.935
4	hot spot on C2	1.852

Notes. C1 and C2 represent component star 1 and 2 respectively.

squared residuals for the best solution of each scenario. It could be seen that the sum of squared residuals of spotted models are remarkably smaller than that of Non-spot model. When finding the converged solutions, we noticed that these two kinds of cool spot models have the similar parameters. The same situation was found with those two kinds of hot spot models. Thus we adopted model 1 and model 4 to give detailed description. The parameters of model 0 (non-spot), model 1 (cool spot) and model 4 (hot spot) are listed in Table 5. The corresponding theoretical light curves of these models are plotted in Figure 4. We can see in this figure that the observed light curves are more perfectly fitted by the hot spot model which reveals that V1799 Ori is a W-type shallow contact binary system with a degree of contact of $f = (\Omega - \Omega_{\rm in})/(\Omega_{\rm out} - \Omega_{\rm in}) = 3.5\% \pm 1.1\%$. The geometrical structure of the binary is shown in Figure 5.

5 CONCLUSION AND DISCUSSION

The deep eclipses in both primary and secondary light minimum which denotes high inclination of the binary system help us to give reliable solutions of the system. Based on the complete BV(RI)$_{\rm c}$ light curves, the photometric solutions for V1799 Ori were carefully derived. We found that V1799 Ori is a extreme-shallow contact binary system with a mass ratio of $q = M_2/M_1 = 1.335 \pm 0.005$ and a degree of contact about $f = 3.5\% \pm 1.1\%$. It is a W-type system of which the less massive component is about 220 K hotter than the more massive one. The asymmetric light curves can be well modeled by employing a hot spot on the primary. Assuming that the primary component is a K0 type main-sequence star, its

Table 5 Photometric Solutions for V1799 Ori from different spot scenarios

Parameters	Model 0 Non-spot	Model 1 Cool spot	Model 4 Hot spot
$q\,(M_2/M_1)$	1.300 ± 0.003	1.300 ± 0.007	1.335 ± 0.005
Ω_{in}	4.2233	4.2233	4.2771
Ω_{out}	3.6571	3.6571	3.7087
T_2 (K)	4805 ± 5	4801 ± 4	4781 ± 4
$i(^\circ)$	89.8 ± 0.9	89.8 ± 0.8	89.7 ± 0.8
$L_1/(L_1+L_2)$ (B)	0.5176 ± 0.0022	0.5196 ± 0.0019	0.5206 ± 0.0017
$L_1/(L_1+L_2)$ (V)	0.5022 ± 0.0018	0.5038 ± 0.0016	0.5033 ± 0.0014
$L_1/(L_1+L_2)$ (R)	0.4900 ± 0.0015	0.4914 ± 0.0015	0.4895 ± 0.0012
$L_1/(L_1+L_2)$ (I)	0.4823 ± 0.0013	0.4835 ± 0.0014	0.4809 ± 0.0011
$\Omega_1 = \Omega_2$	4.1763 ± 0.0066	4.1695 ± 0.0119	4.2572 ± 0.0064
$r_1(pole)$	0.3395 ± 0.0008	0.3403 ± 0.0015	0.3343 ± 0.0008
$r_1(side)$	0.3564 ± 0.0010	0.3573 ± 0.0018	0.3504 ± 0.0010
$r_1(back)$	0.3910 ± 0.0015	0.3924 ± 0.0029	0.3833 ± 0.0016
$r_2(pole)$	0.3832 ± 0.0008	0.3839 ± 0.0014	0.3824 ± 0.0008
$r_2(side)$	0.4048 ± 0.0010	0.4058 ± 0.0017	0.4037 ± 0.0010
$r_2(back)$	0.4372 ± 0.0014	0.4385 ± 0.0025	0.4345 ± 0.0014
$f(\%)$	8.3 ± 1.2	9.5 ± 2.1	3.5 ± 1.1
$\theta_s(^\circ)$	–	83.1(trial)	74.5(trial)
$\psi_s(^\circ)$	–	262 ± 17	246 ± 10
$r_s(^\circ)$	–	16.6 ± 6.1	10.8 ± 5.9
T_s/T_*	–	0.88 ± 0.11	1.20 ± 0.11
$\Sigma w_i(O-C)_i^2$	0.002854	0.002191	0.001852

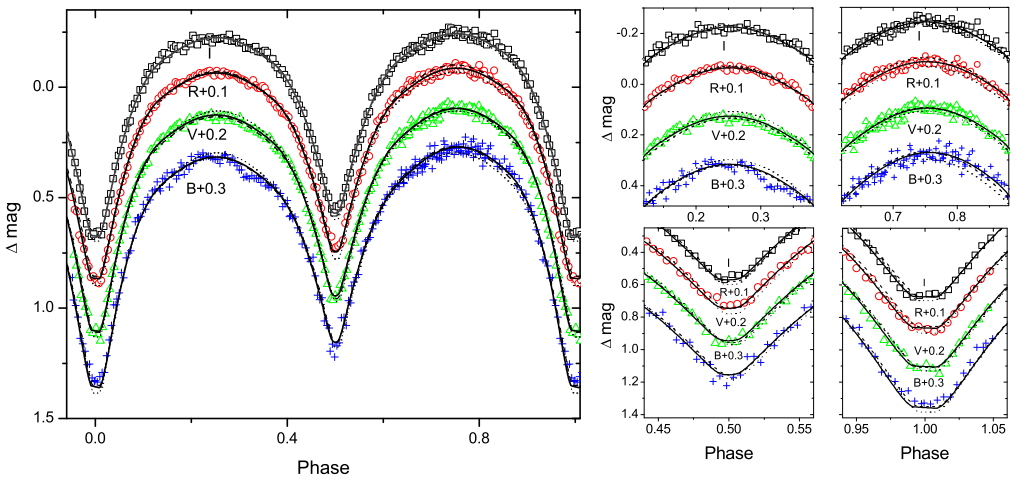

Fig. 4 Observed and theoretical light curves (lines) of V1799 Ori. Different colors of symbols stand for different bands observations. The solid line, dash line and dotted line denote theoretical light curves calculated with hot spot model 4, cool spot model 1 and non-spot model 0, respectively. Left panel: the complete light curves. Right panels: the enlarged small part of the left panel at minimum and maximum phases.

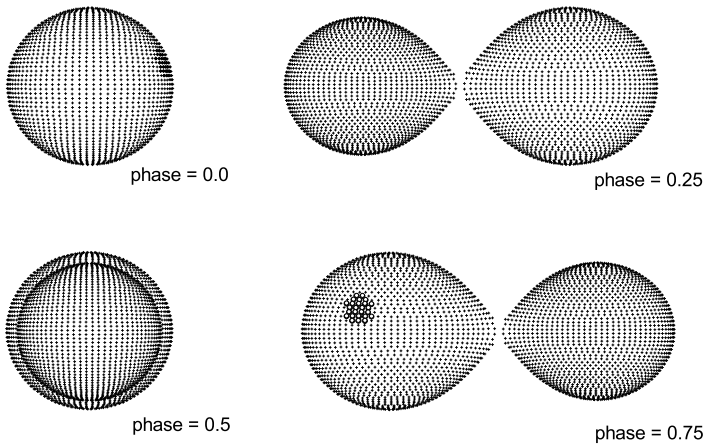

Fig. 5 Geometrical structure of V1799 Ori at phases 0.0, 0.25, 0.5, and 0.75 respectively.

mass was roughly estimated to be $M_2 = 0.80\ \mathrm{M}_\odot$ (Cox 2000). Then the mass the other component was estimated to be $M_1 = 0.60\ \mathrm{M}_\odot$ by using the derived mass ratio.

The photometric solution is in good agreement with that given by Samec et al. (2010) except for the configuration of the star spots. This can be explained by the activity of the components. The solar-like activities on the surface of the binaries are expected to change with time, which would cause different patterns of star spots. When examining the light curves obtained by Samec et al., we found their shapes are slightly different from ours. The difference between the two maximum in their light curves are about 0.03 mag. (B,V), 0.02 mag (R), and 0.01 mag. (I), which are distinctively smaller than that in the newly obtained light curves (see Table 4). This further confirms that the binary is highly active at present.

Based on the analysis of the O-C diagram (Figure 2), a general trend of long-term period increase at a rate of $1.8(\pm0.6) \times 10^{-8}$ days·yr^{-1} was derived. Although the period increase is insignificant (close to the error), it is no doubt a small one compared with other shallow contact binaries (see Table 7 in the paper Zhu et al. 2010). This is in accord with the exceptional low degree of contact, which also agrees that the period-increased system usually have a lower degree of contact (Zhu et al. 2010). The long-term period increase, together with the exceptional low degree of contact, suggests that the binary may be at a critical stage which is predicted by the TRO theory.

If the period variation is caused by a conservative mass transfer, then using the well-known equation

$$\frac{\dot{P}}{P} = 3\frac{\dot{M}_2}{M_2}(\frac{M_2}{M_1} - 1), \tag{6}$$

the mass transfer rate is estimated to be $\mathrm{d}M_2/\mathrm{d}t = 1.4(\pm0.5) \times 10^{-8}\ \mathrm{M}_\odot\cdot\mathrm{yr}^{-1}$. However, the real mass transfer rate may be quite different from this value because of the contribution of angular momentum loss (AML) process (Rahunen 1981; Qian et al. 2013). In addition, it is possible that the long-term increase may be only one part of a long cyclic oscillation. More observations are needed to clarify the nature of the period variation.

Acknowledgements This work was partly supported by the Chinese Natural Science Foundation (Nos. 11133007 and 11325315). New CCD photometric observations of V1799 Ori were obtained with the 1.0-m telescope at Yunnan Observatories.

References

Akerlof, C., Amrose, S., Balsano, R., et al. 2000, AJ, 119, 1901
Alfonso-Garzón, J., Domingo, A., Mas-Hesse, J. M., & Giménez, A. 2012, A&A, 548, A79
Binnendijk, L. 1970, Vistas in Astronomy, 12, 217
Bradstreet, D. H. 1985, ApJS, 58, 413
Cox, A. N. 2000, Allen's Astrophysical Quantities(4th ed.; New York: Springer)
Diethelm, R. 2009, Information Bulletin on Variable Stars, 5871, 1
Diethelm, R. 2010, Information Bulletin on Variable Stars, 5920, 1
Diethelm, R. 2011, Information Bulletin on Variable Stars, 5960, 1
Diethelm, R. 2012, Information Bulletin on Variable Stars, 6029, 1
Diethelm, R. 2013, Information Bulletin on Variable Stars, 6042, 1
Flannery, B. P. 1976, ApJ, 205, 217
Hanley, C. M., & Shapley, H. 1940, Harvard College Observatory Bulletin, 913, 9
Hoffman, D. I., Harrison, T. E., & McNamara, B. J. 2009, AJ, 138, 466
2006, Information Bulletin on Variable Stars, 5699, 1
Lucy, L. B. 1967, ZAp, 65, 89
Lucy, L. B. 1976, ApJ, 205, 208
Milone, E. F. 1968, The Astronomical Journal Supplement, 73, 26
Nelson, R. H. 2010, Information Bulletin on Variable Stars, 5929, 1
O'Connell, D. J. K. 1951, Publications of the Riverview College Observatory, 2, 85
O'Connell, D. J. K. 1951, MNRAS, 111, 642
Qian, S.-B., Liu, N.-P., Liao, W.-P., et al. 2013, AJ, 146, 38
Rahunen, T. 1981, A&A, 102, 81
Robertson, J. A., & Eggleton, P. P. 1977, MNRAS, 179, 359
Ruciński, S. M. 1969, Acta Astronomica, 19, 245
Rucinski, S. M. 1974, Acta Astronomica, 24, 119
Samec, R. G., Melton, R. A., Figg, E. R., et al. 2010, The Observatory, 130, 364
van Hamme, W. 1993, AJ, 106, 2096
Wilson, R. E. 1979, ApJ, 234, 1054
Wilson, R. E. 1990, ApJ, 356, 613
Wilson, R. E. 1994, PASP, 106, 921
Wilson, R. E., & Devinney, E. J. 1971, ApJ, 166, 605
Wilson, R. E. & Van Hamme, W. 2003, Computing Binary Stars Observables (4th ed. of the W-D program), ftp://ftp.astro.ufl.edu/pub/wilson/lcdc2003
Zhou, A.-Y., Jiang, X.-J., Zhang, Y.-P., & Wei, J.-Y. 2009, Research in Astronomy and Astrophysics, 9, 349
Zhu, L., Qian, S.-B., Mikulášek, Z., et al. 2010, AJ, 140, 215

Appendix A:

Table A.1: The B band original data of V1799 Ori observed in 2012 (Hel. JD 2,456,200+).

Hel. JD	Δm	Hel. JD	Δm	Hel. JD	Δm	Hel. JD	Δm	Hel. JD	Δm
76.9944	.151	77.0629	.090	77.1314	.253	77.1998	.111	77.2693	.315
76.9958	.074	77.0643	.095	77.1328	.198	77.2012	.132	77.2707	.310
76.9972	.132	77.0657	.146	77.1342	.210	77.2026	.113	77.2721	.304
76.9986	.092	77.0671	.114	77.1356	.170	77.2040	.147	77.2735	.264
77.0000	.098	77.0685	.165	77.1370	.162	77.2054	.143	77.2749	.235
77.0014	.085	77.0699	.200	77.1384	.128	77.2060	.154	77.2763	.207
77.0028	.098	77.0713	.184	77.1398	.159	77.2074	.152	77.2777	.187
77.0042	.027	77.0727	.252	77.1403	.170	77.2088	.142	77.2791	.186
77.0056	.089	77.0741	.237	77.1417	.112	77.2102	.156	77.2805	.150
77.0070	.036	77.0746	.263	77.1431	.115	77.2116	.194	77.2819	.162
77.0084	.083	77.0760	.280	77.1445	.088	77.2130	.181	77.2824	.139
77.0090	.053	77.0774	.345	77.1459	.152	77.2144	.241	77.2838	.137
77.0104	.047	77.0788	.397	77.1473	.086	77.2158	.228	77.2862	.107
77.0118	.022	77.0802	.405	77.1487	.084	77.2172	.213	77.2876	.136
77.0132	.010	77.0816	.481	77.1501	.115	77.2186	.286	77.2890	.075
77.0146	.068	77.0830	.487	77.1515	.100	77.2191	.281	77.2904	.107
77.0160	.000	77.0844	.509	77.1529	.042	77.2205	.295	77.2918	.072
77.0174	.025	77.0858	.565	77.1534	.061	77.2219	.288	77.2932	.062
77.0188	.023	77.0872	.561	77.1548	.095	77.2233	.337	77.2946	.053
77.0202	-.003	77.0878	.663	77.1562	.056	77.2247	.359	77.2960	.067
77.0216	-.015	77.0892	.688	77.1576	.071	77.2261	.410	77.2974	.056
77.0221	-.040	77.0906	.741	77.1590	.013	77.2285	.428	77.2988	.065
77.0235	-.020	77.0920	.837	77.1604	.044	77.2299	.476	77.3002	.058
77.0249	-.016	77.0934	.862	77.1618	.032	77.2313	.490	77.3007	.050
77.0263	-.034	77.0948	.896	77.1632	.004	77.2327	.469	77.3021	.012
77.0277	-.034	77.0962	.957	77.1646	.017	77.2341	.554	77.3035	-.034
77.0291	-.032	77.0976	.954	77.1660	-.003	77.2355	.641	77.3049	.014
77.0305	-.039	77.0990	1.016	77.1666	.016	77.2369	.662	77.3063	-.036
77.0319	-.013	77.1004	1.033	77.1680	.014	77.2383	.654	77.3077	.017
77.0333	.001	77.1009	1.028	77.1694	.012	77.2397	.759	77.3091	.002
77.0347	-.074	77.1023	1.035	77.1708	.016	77.2411	.779	77.3105	.030
77.0352	.002	77.1037	1.011	77.1722	.023	77.2425	.790	77.3119	-.057
77.0366	-.005	77.1051	.991	77.1736	.028	77.2430	.896	77.3133	.014
77.0380	-.028	77.1065	.991	77.1750	.027	77.2444	.863	77.3139	-.002
77.0394	.017	77.1079	.915	77.1764	.046	77.2458	.921	77.3153	-.014
77.0408	.002	77.1093	.844	77.1778	.016	77.2472	.870	77.3167	-.023
77.0422	-.033	77.1107	.778	77.1792	.008	77.2486	.857	77.3181	.005
77.0436	-.020	77.1121	.685	77.1797	.006	77.2500	.743	77.3195	-.023
77.0450	-.047	77.1135	.685	77.1811	.021	77.2514	.742	77.3209	-.010
77.0464	.017	77.1140	.659	77.1825	.040	77.2528	.778	77.3223	-.006
77.0478	.002	77.1154	.631	77.1839	.020	77.2542	.667	77.3237	-.044
77.0484	-.021	77.1168	.539	77.1853	.041	77.2556	.676	77.3251	-.025
77.0498	-.035	77.1182	.563	77.1867	.056	77.2561	.600	77.3265	-.021
77.0512	.023	77.1196	.472	77.1881	.074	77.2575	.582	77.3270	-.009
77.0526	.025	77.1210	.451	77.1895	.075	77.2589	.562	77.3284	-.054

Table A.1: (continued)

Hel. JD	Δm	Hel. JD	Δm	Hel. JD	Δm	Hel. JD	Δm	Hel. JD	Δm
77.0540	.059	77.1224	.441	77.1909	.108	77.2603	.548	77.3298	-.065
77.0554	.044	77.1238	.384	77.1923	.103	77.2617	.442	77.3312	-.031
77.0568	.070	77.1252	.309	77.1928	.105	77.2631	.438	77.3326	-.009
77.0582	.025	77.1266	.292	77.1942	.114	77.2645	.397	77.3340	.005
77.0596	.068	77.1272	.290	77.1956	.101	77.2659	.390	77.3354	.057
77.0610	.081	77.1286	.284	77.1970	.112	77.2673	.380	77.3368	.024
77.0615	.059	77.1300	.230	77.1984	.114	77.2687	.341		

Table A.2: The V band original data of V1799 Ori observed in 2012 (Hel. JD 2,456,200+).

Hel. JD	Δm	Hel. JD	Δm	Hel. JD	Δm	Hel. JD	Δm	Hel. JD	Δm
76.9949	.004	77.0634	.017	77.1318	.149	77.2003	.007	77.2697	.234
76.9963	.063	77.0648	.051	77.1332	.143	77.2017	.015	77.2711	.201
76.9977	.012	77.0662	.066	77.1346	.083	77.2031	.020	77.2725	.168
76.9991	.023	77.0676	.064	77.1360	.086	77.2045	.036	77.2739	.145
77.0005	.017	77.0690	.091	77.1374	.069	77.2064	.026	77.2753	.137
77.0019	-.050	77.0704	.116	77.1388	.051	77.2078	.042	77.2767	.138
77.0033	-.035	77.0718	.133	77.1408	.031	77.2092	.068	77.2781	.114
77.0047	-.020	77.0732	.135	77.1422	.026	77.2106	.081	77.2795	.067
77.0061	-.017	77.0751	.223	77.1436	.035	77.2120	.092	77.2809	.067
77.0075	-.058	77.0765	.241	77.1450	.017	77.2134	.087	77.2829	.024
77.0094	-.023	77.0779	.228	77.1464	-.003	77.2149	.110	77.2843	.039
77.0108	-.055	77.0793	.294	77.1478	-.008	77.2163	.129	77.2867	.028
77.0122	-.040	77.0807	.339	77.1492	-.021	77.2177	.127	77.2881	.003
77.0136	-.059	77.0821	.366	77.1506	-.029	77.2196	.153	77.2895	-.001
77.0150	-.033	77.0835	.395	77.1520	-.037	77.2210	.183	77.2909	.005
77.0164	-.086	77.0849	.445	77.1539	-.024	77.2224	.209	77.2923	-.014
77.0178	-.049	77.0863	.474	77.1553	-.012	77.2238	.229	77.2937	-.020
77.0192	-.057	77.0882	.560	77.1567	-.046	77.2252	.252	77.2951	-.023
77.0206	-.095	77.0896	.609	77.1581	-.060	77.2266	.268	77.2965	-.035
77.0226	-.118	77.0910	.653	77.1595	-.041	77.2289	.353	77.2979	-.049
77.0240	-.099	77.0924	.742	77.1609	-.044	77.2303	.371	77.2993	-.072
77.0254	-.108	77.0938	.759	77.1623	-.063	77.2317	.408	77.3012	-.059
77.0268	-.117	77.0952	.795	77.1637	-.069	77.2331	.439	77.3026	-.087
77.0282	-.092	77.0966	.822	77.1651	-.070	77.2345	.465	77.3040	-.073
77.0296	-.091	77.0980	.900	77.1670	-.065	77.2359	.509	77.3054	-.086
77.0310	-.117	77.0994	.914	77.1684	-.070	77.2373	.548	77.3068	-.075
77.0324	-.099	77.1014	.891	77.1698	-.059	77.2387	.578	77.3082	-.089
77.0338	-.102	77.1028	.919	77.1712	-.082	77.2401	.628	77.3096	-.104
77.0357	-.087	77.1042	.949	77.1726	-.064	77.2415	.692	77.3110	-.113
77.0371	-.092	77.1056	.887	77.1740	-.045	77.2435	.759	77.3124	-.115
77.0385	-.107	77.1070	.826	77.1754	-.066	77.2449	.765	77.3143	-.132
77.0399	-.107	77.1084	.761	77.1768	-.061	77.2463	.743	77.3157	-.117
77.0413	-.055	77.1098	.715	77.1782	-.069	77.2477	.753	77.3171	-.114
77.0427	-.115	77.1112	.647	77.1802	-.069	77.2491	.696	77.3185	-.099
77.0441	-.094	77.1126	.615	77.1816	-.046	77.2505	.713	77.3199	-.103

Table A.2: (continued)

Hel. JD	Δm	Hel. JD	Δm	Hel. JD	Δm	Hel. JD	Δm	Hel. JD	Δm
77.0455	-.086	77.1145	.544	77.1830	-.068	77.2519	.657	77.3213	-.090
77.0469	-.075	77.1159	.495	77.1844	-.057	77.2533	.628	77.3227	-.119
77.0488	-.078	77.1173	.451	77.1858	-.046	77.2547	.564	77.3242	-.102
77.0502	-.062	77.1187	.422	77.1872	-.041	77.2566	.500	77.3256	-.106
77.0516	-.059	77.1201	.380	77.1886	-.065	77.2580	.505	77.3275	-.113
77.0530	-.037	77.1215	.330	77.1900	-.031	77.2594	.443	77.3289	-.081
77.0544	-.028	77.1229	.307	77.1914	-.027	77.2608	.411	77.3303	-.101
77.0558	-.020	77.1243	.285	77.1933	-.014	77.2622	.373	77.3317	-.091
77.0572	.008	77.1257	.248	77.1947	-.011	77.2636	.349	77.3331	-.080
77.0586	-.003	77.1276	.198	77.1961	-.007	77.2650	.316	77.3345	-.085
77.0600	-.003	77.1290	.186	77.1975	-.014	77.2664	.271	77.3359	-.080
77.0620	.002	77.1304	.159	77.1989	.006	77.2678	.262	77.3373	-.046

Table A.3: The R band original data of V1799 Ori observed in 2012 (Hel. JD 2,456,200+).

Hel. JD	Δm	Hel. JD	Δm	Hel. JD	Δm	Hel. JD	Δm	Hel. JD	Δm
76.9952	-.069	77.0637	-.059	77.1322	.047	77.2006	-.096	77.2701	.118
76.9966	-.084	77.0651	-.048	77.1336	.017	77.2020	-.106	77.2715	.054
76.9980	-.082	77.0665	-.044	77.1350	-.012	77.2034	-.097	77.2729	.047
76.9994	-.078	77.0679	-.019	77.1364	-.010	77.2048	-.076	77.2743	.033
77.0008	-.132	77.0693	.019	77.1378	-.022	77.2068	-.046	77.2757	.044
77.0022	-.121	77.0707	.029	77.1392	-.049	77.2082	-.043	77.2771	.016
77.0036	-.122	77.0721	.054	77.1411	-.065	77.2096	-.024	77.2785	-.017
77.0050	-.133	77.0735	.072	77.1425	-.076	77.2110	-.009	77.2799	-.037
77.0064	-.156	77.0754	.115	77.1439	-.084	77.2124	-.011	77.2813	-.050
77.0078	-.140	77.0768	.125	77.1453	-.082	77.2138	.016	77.2832	-.070
77.0098	-.124	77.0782	.171	77.1467	-.098	77.2152	.019	77.2846	-.066
77.0112	-.158	77.0796	.184	77.1481	-.084	77.2166	.025	77.2870	-.088
77.0126	-.154	77.0810	.225	77.1495	-.124	77.2180	.036	77.2884	-.082
77.0140	-.134	77.0824	.279	77.1509	-.117	77.2199	.077	77.2898	-.110
77.0154	-.148	77.0838	.295	77.1523	-.117	77.2213	.090	77.2912	-.100
77.0168	-.175	77.0852	.329	77.1542	-.124	77.2227	.114	77.2926	-.125
77.0182	-.151	77.0866	.397	77.1556	-.113	77.2241	.137	77.2940	-.117
77.0196	-.152	77.0886	.454	77.1570	-.127	77.2255	.170	77.2954	-.125
77.0210	-.178	77.0900	.463	77.1584	-.143	77.2269	.202	77.2968	-.132
77.0229	-.192	77.0914	.570	77.1598	-.141	77.2293	.233	77.2982	-.141
77.0243	-.191	77.0928	.591	77.1612	-.153	77.2307	.279	77.2996	-.159
77.0257	-.183	77.0942	.631	77.1626	-.151	77.2321	.299	77.3015	-.150
77.0271	-.179	77.0956	.690	77.1640	-.164	77.2335	.351	77.3029	-.167
77.0285	-.210	77.0970	.712	77.1654	-.158	77.2349	.355	77.3043	-.158
77.0299	-.195	77.0984	.760	77.1674	-.166	77.2363	.425	77.3057	-.169
77.0313	-.182	77.0998	.756	77.1688	-.171	77.2377	.448	77.3071	-.178
77.0327	-.201	77.1017	.772	77.1702	-.175	77.2391	.501	77.3085	-.168
77.0341	-.198	77.1031	.788	77.1716	-.163	77.2405	.544	77.3099	-.174
77.0360	-.187	77.1045	.774	77.1730	-.152	77.2419	.567	77.3113	-.174
77.0374	-.170	77.1059	.733	77.1744	-.174	77.2438	.577	77.3127	-.182

Table A.3: (continued)

Hel. JD	Δm	Hel. JD	Δm	Hel. JD	Δm	Hel. JD	Δm	Hel. JD	Δm
77.0388	-.151	77.1073	.678	77.1758	-.158	77.2452	.630	77.3147	-.169
77.0402	-.144	77.1087	.636	77.1772	-.153	77.2466	.625	77.3161	-.184
77.0416	-.177	77.1101	.580	77.1786	-.171	77.2480	.618	77.3175	-.183
77.0430	-.200	77.1115	.524	77.1805	-.164	77.2494	.610	77.3189	-.184
77.0444	-.168	77.1129	.464	77.1819	-.154	77.2508	.592	77.3203	-.176
77.0458	-.175	77.1148	.417	77.1833	-.159	77.2522	.515	77.3217	-.193
77.0472	-.145	77.1162	.377	77.1847	-.158	77.2536	.486	77.3231	-.179
77.0492	-.149	77.1176	.325	77.1861	-.152	77.2550	.442	77.3245	-.196
77.0506	-.129	77.1190	.299	77.1875	-.144	77.2569	.384	77.3259	-.180
77.0520	-.176	77.1204	.261	77.1889	-.135	77.2583	.379	77.3278	-.158
77.0534	-.119	77.1218	.207	77.1903	-.135	77.2597	.325	77.3292	-.165
77.0548	-.110	77.1232	.165	77.1917	-.130	77.2611	.288	77.3306	-.164
77.0562	-.091	77.1246	.154	77.1936	-.108	77.2625	.284	77.3320	-.160
77.0576	-.083	77.1260	.126	77.1950	-.115	77.2639	.230	77.3334	-.162
77.0590	-.100	77.1280	.100	77.1964	-.132	77.2653	.206	77.3348	-.157
77.0604	-.085	77.1294	.064	77.1978	-.109	77.2667	.212	77.3362	-.156
77.0623	-.067	77.1308	.057	77.1992	-.097	77.2681	.144	77.3376	-.133

Table A.4: The I band original data of V1799 Ori observed in 2012 (Hel. JD 2,456,200+).

Hel. JD	Δm	Hel. JD	Δm	Hel. JD	Δm	Hel. JD	Δm	Hel. JD	Δm
76.9954	-.131	77.0639	-.130	77.1324	-.065	77.2009	-.160	77.2703	.024
76.9968	-.133	77.0653	-.116	77.1338	-.057	77.2023	-.157	77.2717	.022
76.9982	-.147	77.0667	-.100	77.1352	-.092	77.2037	-.167	77.2731	.008
76.9997	-.165	77.0681	-.105	77.1366	-.083	77.2051	-.158	77.2745	-.026
77.0011	-.156	77.0695	-.073	77.1380	-.098	77.2070	-.130	77.2759	-.041
77.0025	-.187	77.0709	-.046	77.1394	-.121	77.2084	-.129	77.2773	-.027
77.0039	-.188	77.0723	-.011	77.1413	-.147	77.2098	-.102	77.2787	-.064
77.0053	-.176	77.0737	-.014	77.1427	-.156	77.2112	-.089	77.2801	-.086
77.0067	-.170	77.0756	.041	77.1441	-.125	77.2126	-.059	77.2815	-.108
77.0081	-.162	77.0770	.056	77.1455	-.151	77.2140	-.079	77.2834	-.138
77.0100	-.225	77.0784	.104	77.1469	-.193	77.2154	-.057	77.2848	-.127
77.0114	-.198	77.0798	.127	77.1483	-.177	77.2168	-.041	77.2872	-.143
77.0128	-.181	77.0812	.175	77.1497	-.186	77.2182	-.018	77.2886	-.164
77.0142	-.194	77.0827	.165	77.1511	-.173	77.2201	.023	77.2900	-.155
77.0156	-.212	77.0841	.235	77.1525	-.186	77.2215	.038	77.2914	-.170
77.0170	-.216	77.0855	.262	77.1545	-.162	77.2229	.056	77.2928	-.165
77.0184	-.210	77.0869	.298	77.1559	-.184	77.2243	.081	77.2942	-.179
77.0198	-.222	77.0888	.341	77.1573	-.198	77.2257	.105	77.2956	-.182
77.0212	-.247	77.0902	.387	77.1587	-.197	77.2271	.118	77.2970	-.187
77.0231	-.243	77.0916	.456	77.1601	-.235	77.2295	.178	77.2984	-.212
77.0245	-.271	77.0930	.512	77.1615	-.220	77.2309	.210	77.2998	-.196
77.0259	-.269	77.0944	.561	77.1629	-.193	77.2323	.237	77.3018	-.209
77.0273	-.258	77.0958	.618	77.1643	-.221	77.2337	.280	77.3032	-.204
77.0287	-.247	77.0972	.660	77.1657	-.223	77.2351	.315	77.3046	-.229
77.0301	-.265	77.0986	.675	77.1676	-.209	77.2365	.343	77.3060	-.234

Table A.4: (continued)

Hel. JD	Δm	Hel. JD	Δm	Hel. JD	Δm	Hel. JD	Δm	Hel. JD	Δm
77.0315	-.237	77.1000	.665	77.1690	-.210	77.2379	.407	77.3074	-.227
77.0329	-.252	77.1019	.655	77.1704	-.227	77.2393	.422	77.3088	-.229
77.0343	-.258	77.1033	.651	77.1718	-.201	77.2407	.481	77.3102	-.232
77.0362	-.233	77.1047	.668	77.1732	-.219	77.2421	.499	77.3116	-.236
77.0376	-.235	77.1061	.629	77.1746	-.217	77.2440	.551	77.3130	-.233
77.0390	-.246	77.1075	.570	77.1760	-.220	77.2454	.569	77.3149	-.247
77.0404	-.257	77.1089	.513	77.1774	-.221	77.2468	.538	77.3163	-.249
77.0418	-.228	77.1103	.482	77.1788	-.225	77.2482	.541	77.3177	-.256
77.0432	-.226	77.1117	.414	77.1807	-.213	77.2496	.529	77.3191	-.235
77.0446	-.235	77.1131	.358	77.1821	-.239	77.2510	.497	77.3205	-.240
77.0461	-.231	77.1151	.309	77.1835	-.209	77.2524	.455	77.3219	-.237
77.0475	-.228	77.1165	.287	77.1849	-.211	77.2538	.410	77.3233	-.226
77.0494	-.224	77.1179	.234	77.1863	-.220	77.2552	.388	77.3247	-.236
77.0508	-.198	77.1193	.187	77.1877	-.202	77.2571	.324	77.3261	-.236
77.0522	-.244	77.1207	.160	77.1891	-.204	77.2585	.298	77.3280	-.214
77.0536	-.203	77.1221	.153	77.1905	-.201	77.2599	.272	77.3294	-.227
77.0550	-.183	77.1235	.095	77.1919	-.177	77.2613	.234	77.3308	-.226
77.0564	-.178	77.1249	.076	77.1939	-.179	77.2627	.210	77.3322	-.212
77.0578	-.156	77.1263	.051	77.1953	-.176	77.2641	.159	77.3336	-.207
77.0592	-.143	77.1282	.011	77.1967	-.171	77.2655	.123	77.3350	-.211
77.0606	-.170	77.1296	.012	77.1981	-.184	77.2669	.111	77.3364	-.200
77.0625	-.133	77.1310	-.029	77.1995	-.162	77.2683	.044	77.3378	-.193